



Contents lists available at ScienceDirect

Chinese Chemical Letters

journal homepage: [www.elsevier.com/locate/cclet](http://www.elsevier.com/locate/cclet)

Communication

# Highly ordered Nb<sub>2</sub>O<sub>5</sub> nanochannel film with rich oxygen vacancies for electrocatalytic N<sub>2</sub> reduction: Inactivation and regeneration of electrode

Jialu Wang<sup>a,b</sup>, Shenghong Kang<sup>a,\*</sup>, Xiaoguang Zhu<sup>a</sup>, Guozhong Wang<sup>a</sup>, Haimin Zhang<sup>a,\*</sup><sup>a</sup> Key Laboratory of Materials Physics, Centre for Environmental and Energy Nanomaterials, Anhui Key Laboratory of Nanomaterials and Nanotechnology, Institute of Solid State Physics, Chinese Academy of Sciences, Hefei 230031, China<sup>b</sup> University of Science and Technology of China, Hefei 230026, China

## ARTICLE INFO

## Article history:

Received 26 September 2020

Received in revised form 19 November 2020

Accepted 11 January 2021

Available online xxx

## Keywords:

Niobium oxide (Nb<sub>2</sub>O<sub>5</sub>)Nitrogen (N<sub>2</sub>) reduction reaction (NRR)

Electrochromism

Oxygen vacancies

Phase transformation

## ABSTRACT

We report the fabrication of highly ordered Nb<sub>2</sub>O<sub>5</sub> nanochannel film (Nb<sub>2</sub>O<sub>5</sub>-NCF) onto niobium foil by an anodization method. After thermal treatment, the obtained Nb<sub>2</sub>O<sub>5</sub>-NCF with rich oxygen vacancies exhibits electrochemical N<sub>2</sub> reduction reaction (NRR) activity with an NH<sub>3</sub> yield rate of  $2.52 \times 10^{-10}$  mol cm<sup>-2</sup> s<sup>-1</sup> and a faradaic efficiency of 9.81% at -0.4 V (vs. RHE) in 0.1 mol/L Na<sub>2</sub>SO<sub>4</sub> electrolyte (pH 3.2). During electrocatalytic NRR, the Nb<sub>2</sub>O<sub>5</sub>-NCF takes place electrochromism (EC), along with a crystalline phase transformation from pseudo hexagonal phase to hexagonal phase owing to H<sup>+</sup> insertion. This results in the reduced NRR activity due to the decrease of oxygen vacancies of hexagonal phase Nb<sub>2</sub>O<sub>5</sub>, which can be readily regenerated by low-temperature thermal treatment or applying an anodic potential, showing superior recycling reproducibility.

© 2021 Chinese Chemical Society and Institute of Materia Medica, Chinese Academy of Medical Sciences. Published by Elsevier B.V. All rights reserved.

Ammonia (NH<sub>3</sub>) as very important chemical has been widely applied in fuel of vehicles, agricultural, plastic and textile industries [1–4]. Although abundant nitrogen (N<sub>2</sub>) exists in the atmosphere (~78%), efficient utilization of N<sub>2</sub> is still very difficult due to high energy barrier for N≡N bond cleavage (~941 kJ/mol), large energy gap (~10.82 eV), and the lowest unoccupied molecular orbital [5]. The synthesis of NH<sub>3</sub> by N<sub>2</sub> hydrogenation is a complex reduction process with multiple reactions [6–8]. Industrially, the NH<sub>3</sub> production from N<sub>2</sub> and H<sub>2</sub> was performed at high temperature (400–600 °C) and pressure (20–40 MPa) by the well-known Haber–Bosch process [9–12], consuming enormous energy and concurrently releasing a large amount of CO<sub>2</sub>. Therefore, development of environmentally friendly NH<sub>3</sub> synthesis techniques at ambient conditions is highly desirable.

Electrocatalytic N<sub>2</sub> reduction reaction (NRR) at ambient conditions has been regarded as a promising NH<sub>3</sub> synthesis method for replacing the traditional energy- and capital-intensive Haber–Bosch process [9–12]. To date, varieties of electrocatalysts have been synthesized and applied in electrocatalytic NRR to synthesize NH<sub>3</sub>, such as noble metal catalysts [13,14], non-precious metal catalysts [15,16] and metal-free carbon catalysts [17–19],

demonstrating high NRR activities. Among non-precious metal catalysts, transition metal oxides have been proven to be efficient catalysts toward electrocatalytic NRR to NH<sub>3</sub>, confirming the oxygen vacancies (V<sub>o</sub>) as the active centers [20–24]. As we know, niobium oxides have become important materials for catalysis applications [25] because of their superior catalytic activity and high physical/chemical stability. Recently, Kong *et al.* [26] reported Nb<sub>2</sub>O<sub>5</sub> nanowires array as high-performance NRR electrocatalyst, demonstrating an NH<sub>3</sub> yield rate of  $1.58 \times 10^{-10}$  mol s<sup>-1</sup> cm<sup>-2</sup> with a Faradaic efficiency (FE) of 2.26%. In their work, this good NRR activity can be ascribed to the important role of (001) facet of Nb<sub>2</sub>O<sub>5</sub>. The Nb<sub>2</sub>O<sub>5</sub> nanofiber with high conductivity was also synthesized by Han and co-workers for electrocatalytic NRR to NH<sub>3</sub> [27], showing an NH<sub>3</sub> yield rate of 43.6 μg h<sup>-1</sup> mg<sub>cat</sub><sup>-1</sup> with an FE of 9.26%. In their study, this high NRR activity is mainly resulted from Nb-edge atoms of Nb<sub>2</sub>O<sub>5</sub> (181) surface to polarize and activate N<sub>2</sub> molecules. It is well known that *pseudo* hexagonal phase Nb<sub>2</sub>O<sub>5</sub> has been confirmed to contain rich V<sub>o</sub> [28], which could be a promising candidate as the electrocatalyst for NRR to NH<sub>3</sub>. In particular, *pseudo* hexagonal phase Nb<sub>2</sub>O<sub>5</sub> nanostructured arrays (*e.g.*, nanochannel array) could provide more excellent electron transfer pathways with exposed V<sub>o</sub> active sites for high-efficiency NRR [29,30].

Herein, highly ordered Nb<sub>2</sub>O<sub>5</sub> nanochannel film (Nb<sub>2</sub>O<sub>5</sub>-NCF) was fabricated on niobium foil substrate by a facile anodization

\* Corresponding authors.

E-mail addresses: [shkang@issp.ac.cn](mailto:shkang@issp.ac.cn) (S. Kang), [zhanghm@issp.ac.cn](mailto:zhanghm@issp.ac.cn) (H. Zhang).

method. After thermal treatment in air, the as-fabricated Nb<sub>2</sub>O<sub>5</sub>-NCF with pseudo hexagonal phase contains rich oxygen vacancy defects, as the free-standing electrode, displaying high electrocatalytic NRR activity with an NH<sub>3</sub> yield rate of  $2.52 \times 10^{-10}$  mol cm<sup>-2</sup> s<sup>-1</sup> and an FE of 9.81% at -0.4 V (vs. RHE) in 0.1 mol/L Na<sub>2</sub>SO<sub>4</sub> solution (pH 3.2). During electrocatalytic NRR, it was found that the crystalline phase transformation of Nb<sub>2</sub>O<sub>5</sub>-NCF from pseudo hexagonal phase to hexagonal phase resulted in the electrochromism (EC) phenomenon and the decrease of NRR activity. This is mainly due to the decrease of V<sub>o</sub> in hexagonal phase Nb<sub>2</sub>O<sub>5</sub>. The used Nb<sub>2</sub>O<sub>5</sub>-NCF electrode can be readily regenerated by low-temperature thermal treatment or applying an anodic potential, regaining high NH<sub>3</sub> yield rate and FE with superior recycling reproducibility.

After anodization, the surface of niobium (Nb) foil showed dark brown and the surface colour of Nb foil became white after further treating in air at 450 °C (Fig. S1 in Supporting information). The XRD patterns (Fig. 1a) of the thermally treated sample exhibit a *pseudo* hexagonal phase (TT-phase) Nb<sub>2</sub>O<sub>5</sub> (JCPDS No. 28-0317) [28]. The SEM images (Figs. 1b and c) show that the surface of the sample possesses porous structure, and a highly ordered nanochannel film with a thickness of ~2.0 μm forms on the Nb foil substrate (denoted as Nb<sub>2</sub>O<sub>5</sub>-NCF). The TEM image and selected area electron diffraction (SAED) patterns of the sample (Fig. 1d) confirm that the nanochannel walls are polycrystalline structure and the lattice fringes with interplanar distance of 3.12 Å can be ascribed to the (100) plane of TT-phase Nb<sub>2</sub>O<sub>5</sub>. The surface survey XPS spectrum of Nb<sub>2</sub>O<sub>5</sub>-NCF sample was provided in Fig. S2a (Supporting information), exhibiting Nb and O elements. The high-resolution Nb 3d XPS spectrum (Fig. S2b in Supporting information) indicates that the Nb 3d peaks at 209.6 and 206.9 eV can be assigned to Nb<sub>2</sub>O<sub>5</sub> [31,32].

In this work, the fabricated Nb<sub>2</sub>O<sub>5</sub>-NCF was directly used as the cathodic electrode for NRR evaluation in 0.1 mol/L Na<sub>2</sub>SO<sub>4</sub> solution (pH 3.2) using an H-type electrochemical cell. The linear sweep voltammograms (LSV) results (Fig. 2a) show that the cathodic current density of Nb<sub>2</sub>O<sub>5</sub>-NCF electrode in N<sub>2</sub>-saturated electrolyte is obviously larger than that obtained in Ar-saturated electrolyte when increasing applied potential from -0.3 V to -0.9 V, confirming good NRR activity of Nb<sub>2</sub>O<sub>5</sub>-NCF. Next, we investigated the influence of applied potential on the NRR performance of Nb<sub>2</sub>O<sub>5</sub>-NCF. During electrocatalytic NRR, the produced NH<sub>3</sub> and/or N<sub>2</sub>H<sub>4</sub> were determined by the indophenol blue [33] and Watt/

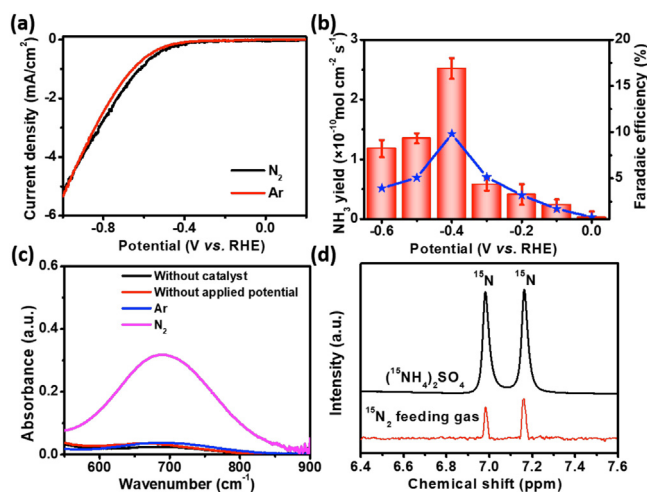


**Fig. 2.** (a) LSV curves under Ar- or N<sub>2</sub>-saturated 0.1 mol/L Na<sub>2</sub>SO<sub>4</sub> solution. (b) NH<sub>3</sub> yield rate and FE of Nb<sub>2</sub>O<sub>5</sub>-NCF at different potentials. (c) UV-vis absorption spectra using the indophenol blue determination method under different conditions. (d) <sup>1</sup>H NMR spectra for <sup>15</sup>NH<sub>4</sub><sup>+</sup> in electrolyte using <sup>15</sup>N<sub>2</sub> as the feeding gas.

Chrissp method [34], respectively. In this work, only NH<sub>3</sub> product can be detected (Fig. S3 in Supporting information) while N<sub>2</sub>H<sub>4</sub> is undetectable (Fig. S4 in Supporting information). Fig. 2b shows the NH<sub>3</sub> yield rate and Faradaic efficiency (FE) of Nb<sub>2</sub>O<sub>5</sub>-NCF at different potentials, and corresponding chronoamperometric curves at each potential are shown in Fig. S5 (Supporting information). According to the UV-vis absorption spectra analysis (Fig. S3a) of NRR samples, the largest NH<sub>3</sub> yield rate can reach  $2.52 \times 10^{-10}$  mol cm<sup>-2</sup> s<sup>-1</sup> with an FE of 9.81% at -0.4 V (vs. RHE) with the NRR time of 60 min (Fig. 2b). When the applied potential is more negative than -0.4 V (vs. RHE), the NRR performance of Nb<sub>2</sub>O<sub>5</sub>-NCF obviously decreases. This is mainly due to the competitive hydrogen evolution reaction (HER) concurrently happened on Nb<sub>2</sub>O<sub>5</sub>-NCF at more negative potentials [27]. To eliminate the environmental interference on the NH<sub>3</sub> yielded during NRR, several control experiments were performed. The results (Fig. 2c) show that no NH<sub>3</sub> product can be detected in 0.1 mol/L Na<sub>2</sub>SO<sub>4</sub> solution without catalyst, with Nb<sub>2</sub>O<sub>5</sub>-NCF but without applied potential, or Ar-saturated electrolyte with Nb<sub>2</sub>O<sub>5</sub>-NCF at -0.4 V (vs. RHE), indicating no environmental interference on the produced NH<sub>3</sub> by NRR process. In contrast, the UV-vis absorption spectra show stronger absorption peak at ~695 nm ascribed to the yielded NH<sub>3</sub> determined by the indophenol blue method. To further confirm this, the isotopic labelling experiments using <sup>15</sup>N<sub>2</sub> as the feeding gas was also conducted. The <sup>1</sup>H nuclear magnetic resonance (NMR) spectra (Fig. 2d) reveal that the chemical shift of doublet coupling can be observed for the NRR sample, due to <sup>15</sup>N in <sup>15</sup>NH<sub>4</sub><sup>+</sup>, suggesting the formed NH<sub>3</sub> indeed originated from the Nb<sub>2</sub>O<sub>5</sub>-NCF catalyzed NRR process.

Subsequently, we evaluated the durability of Nb<sub>2</sub>O<sub>5</sub>-NCF electrode for NRR. It was found that the yielded NH<sub>3</sub> amount during NRR initially rapidly increased. After 20 min, the increase trend of NH<sub>3</sub> yield became slow (Fig. S6 in Supporting information). This results in an initial increase then decrease of NH<sub>3</sub> yield rate, and the largest NH<sub>3</sub> yield rate was obtained to be  $3.38 \times 10^{-10}$  mol cm<sup>-2</sup> s<sup>-1</sup> with an FE of 11.2% at -0.4 V (vs. RHE) (Fig. 3a) when NRR time of 20 min. The above experimental results suggested that the NRR activity of Nb<sub>2</sub>O<sub>5</sub>-NCF decreased after 20 min of reaction, which deserves a further investigation. During electrocatalytic NRR, the Nb<sub>2</sub>O<sub>5</sub> electrode was found to transform to NbO<sub>2</sub> species from XRD results (Fig. 3b), and electrochromism (EC) phenomenon was also observed, namely, the electrode surface color changed from white to dark with NRR time (Fig. 3c). This is mainly

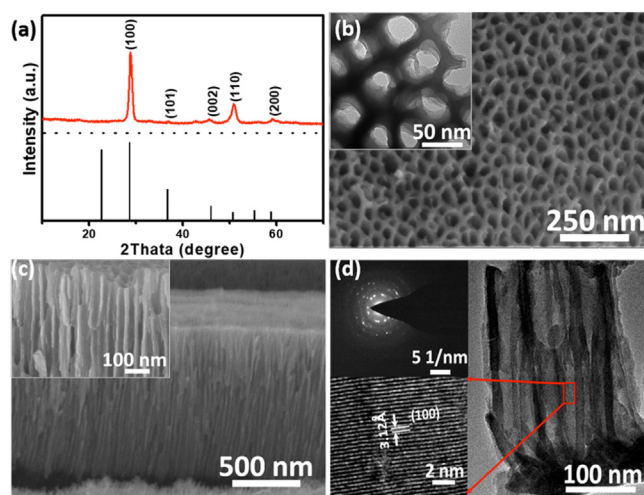


**Fig. 1.** (a) XRD pattern of Nb<sub>2</sub>O<sub>5</sub>-NCF. (b) Surface and (c) cross-sectional SEM images of Nb<sub>2</sub>O<sub>5</sub>-NCF. (d) TEM image and selected area electron diffraction (SAED) patterns for Nb<sub>2</sub>O<sub>5</sub>-NCF.

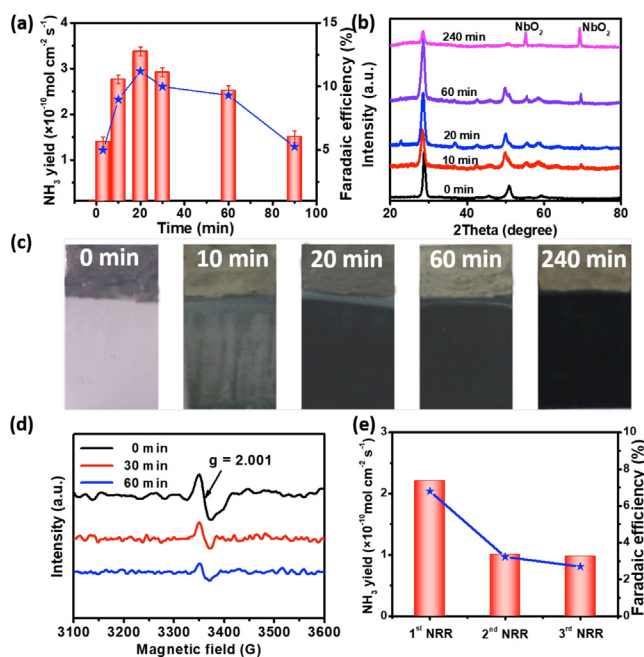


**Fig. 3.** (a) Time-dependence  $\text{NH}_3$  yield rate and FE during continuous NRR. (b) XRD patterns at different times during NRR. (c) The color change of  $\text{Nb}_2\text{O}_5$ -NCF with different reaction times during NRR. (d) EPR spectroscopy of  $\text{V}_o$  under different NRR times. (e) Recycling experiments using the used  $\text{Nb}_2\text{O}_5$ -NCF electrode with fresh 0.1 mol/L  $\text{Na}_2\text{SO}_4$  electrolyte after 20 min of NRR for each cycle.

attributed to  $\text{H}^+$  ions insertion into the interlayer spacing of TT-phase  $\text{Nb}_2\text{O}_5$ , resulting in the crystalline phase transformation of  $\text{Nb}_2\text{O}_5$  from TT-phase to T-phase, concurrently accompanied by part of  $\text{Nb}^{5+}$  reduction to  $\text{Nb}^{4+}$ , thus the generation of EC phenomenon [35]. Seen from the XRD results of  $\text{Nb}_2\text{O}_5$ -NCF electrode with NRR time (Fig. 3b), compared to the pristine  $\text{Nb}_2\text{O}_5$ -NCF, the (100) diffraction peaks of  $\text{Nb}_2\text{O}_5$ -NCF with different NRR times apparently shift toward low angel direction in the XRD patterns, suggesting  $\text{H}^+$  ions insertion into interlayer spacing of  $\text{Nb}_2\text{O}_5$  [36]. As we know, TT-phase  $\text{Nb}_2\text{O}_5$  possesses more oxygen vacancies ( $\text{V}_o$ ) than T-phase  $\text{Nb}_2\text{O}_5$  [28]. These oxygen vacancies have been proven to be the catalytic active sites for  $\text{N}_2$  adsorption, activation and hydrogenation [26,27]. The  $\text{N}_2$  firstly adsorbed on  $\text{V}_o$  sites of  $\text{Nb}_2\text{O}_5$ , and  $\text{V}_o$ -induced bands in  $\text{Nb}_2\text{O}_5$  concurrently provided defect states for trapping excited electrons. Then these electrons were transferred and exchanged to the empty antibonding orbitals ( $p^*$ ) of the adsorbed  $\text{N}_2$ . These adsorbed  $\text{N}_2$  ( $\text{NN}^*$ ) would be severely weakened and exhibited high activation due to the electron injection. It is conducive to hydrogenation for the  $\text{N}\equiv\text{N}$  bond to  $\text{NH}_3$ . During NRR, the crystalline phase transformation from TT-phase to T-phase leads to the decrease of  $\text{V}_o$  concentration in  $\text{Nb}_2\text{O}_5$ , thus the decreased NRR performance.

Fig. 3d shows the electron paramagnetic resonance (EPR) spectroscopy of  $\text{Nb}_2\text{O}_5$ -NCF with different NRR times. In comparison with the pristine  $\text{Nb}_2\text{O}_5$ -NCF, the  $\text{V}_o$  concentration in  $\text{Nb}_2\text{O}_5$  obviously decreased with the NRR time, primarily owing to  $\text{H}^+$  ions occupying the  $\text{V}_o$  sites thus resulting in the reduced active sites for  $\text{N}_2$  adsorption and activation.

After 20 min of NRR, we replaced fresh 0.1 mol/L  $\text{Na}_2\text{SO}_4$  electrolyte and conducted the recycling experiments using the used  $\text{Nb}_2\text{O}_5$ -NCF electrode and obtained obviously decreased NRR performance (Fig. 3e, each recycling experiment of 20 min). The above results further confirmed that with NRR time, the formation of T-phase  $\text{Nb}_2\text{O}_5$  results in the decrease of  $\text{V}_o$  concentration, thus the reduced NRR performance. How to regenerate the electrode with high NRR activity is therefore critically important. We carried

out the cyclic voltammetry (CV) experiments in 0.1 mol/L  $\text{Na}_2\text{SO}_4$  electrolyte in the potential range from  $-1.2$  V to  $1.2$  V (vs. RHE). The results (Fig. S7 in Supporting information) demonstrated that the oxidation peak lies at  $\sim -0.5$  V (vs. RHE), corresponding to the extraction of  $\text{H}^+$  ions from the interlayer spacing of  $\text{Nb}_2\text{O}_5$ . The cathodic current density has a slight increase with the cycling number for  $\text{Nb}_2\text{O}_5$ -NCF and almost unchanged until 25<sup>th</sup> cycle, exhibiting an increased capacity for  $\text{H}^+$  ions insertion. The chronoamperometric measurements were performed by applying potentials of 0.6 and  $-0.6$  V (vs. RHE) for 100 s. The comparison between the anodic and cathodic current intensities indicates a faster kinetic extraction than the insertion process, exhibiting an approximate bleaching time of 15 s while the colored time of 20 s (Fig. 4a). The reversible EC results mean that the used  $\text{Nb}_2\text{O}_5$ -NCF for NRR may be regenerated to recover its high NRR activity. For this, we tried to apply an anodic potential to realize this. As expected, when an anodic potential of 1.0 V (vs. RHE) was applied to the used  $\text{Nb}_2\text{O}_5$ -NCF electrode for 5 min, the T-phase  $\text{Nb}_2\text{O}_5$  with part of  $\text{Nb}^{4+}$  can be readily transformed to TT-phase  $\text{Nb}_2\text{O}_5$  (curve II in Fig. 4b). This means that high NRR performance may be recovered by using the TT-phase  $\text{Nb}_2\text{O}_5$  with more  $\text{V}_o$  sites. Utilizing such regeneration approach, the  $\text{Nb}_2\text{O}_5$ -NCF electrode displays superior recycling reproducibility with high  $\text{NH}_3$  yield rate and current efficiency (Fig. 4c).

Furthermore, we found that low-temperature treatment approach ( $60^\circ\text{C}$  for 0.5 h) is also feasible for regeneration of the used  $\text{Nb}_2\text{O}_5$ -NCF electrode for high-performance NRR (curve III in Fig. 4b). The recycling reproducibility with high  $\text{NH}_3$  yield rate and current efficiency was shown in Fig. 4d. The EPR measurements of  $\text{Nb}_2\text{O}_5$ -NCF sample after 120 min NRR and subsequently low temperature annealing results also confirm this (Fig. S8 in Supporting information).

In summary, highly ordered  $\text{Nb}_2\text{O}_5$  nanochannel film ( $\text{Nb}_2\text{O}_5$ -NCF) with rich  $\text{V}_o$  was fabricated on niobium foil substrate by a facile anodization method. As a free-standing electrode for NRR, the  $\text{Nb}_2\text{O}_5$ -NCF demonstrated high electrocatalytic activity toward  $\text{NH}_3$  synthesis. However, the NRR activity of  $\text{Nb}_2\text{O}_5$ -NCF decreased when the reaction time was over 20 min, due to a crystalline phase transformation of  $\text{Nb}_2\text{O}_5$  from TT-phase to T-phase, resulting in the decrease of  $\text{V}_o$  concentration in  $\text{Nb}_2\text{O}_5$ , thus the reduced active sites for  $\text{N}_2$  adsorption and activation. However, the used  $\text{Nb}_2\text{O}_5$ -NCF with decreased NRR activity could be regenerated by applying an anodic potential

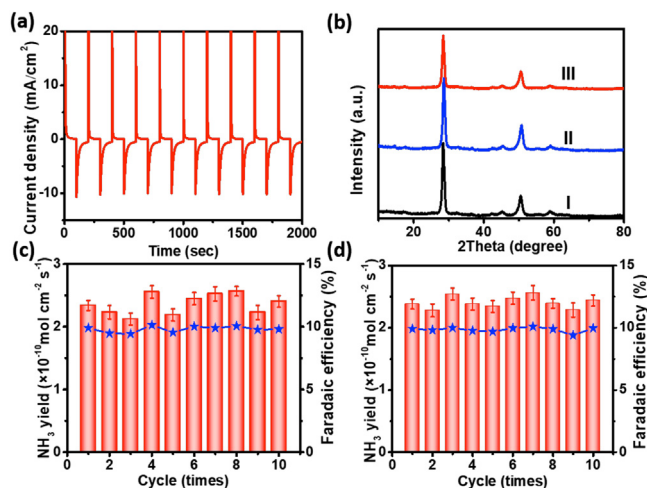


**Fig. 4.** (a) Chronoamperometric (CA) curves of  $\text{Nb}_2\text{O}_5$ -NCF for electrochromism (EC). (b) XRD patterns of  $\text{Nb}_2\text{O}_5$ -NCF before (curve I) and after NRR with anodizing activation (curve II) and low temperature annealing activation (curve III). Recycling test of NRR for  $\text{Nb}_2\text{O}_5$ -NCF electrode by (c) anodizing activation and (d) low temperature annealing activation.

or low-temperature thermal treatment approach, indicating superior recycling reproducibility with high  $\text{NH}_3$  yield rate and current efficiency. This work provides an efficient solution to the inactivation issue of an electrocatalyst for high-performance NRR to  $\text{NH}_3$ .

### Declaration of competing interest

The authors report no declarations of interest.

### Acknowledgments

This work is financially supported by the National Key Research and Development Program of China (No. 2017YFA0207203) and the Natural Science Foundation of China (No. 51872292).

### Appendix A. Supplementary data

Supplementary material related to this article can be found, in the online version, at doi:<https://doi.org/10.1016/j.ccllet.2021.01.020>.

### References

- [1] V. Smil, *Nature* 400 (1999) 415–415.
- [2] V. Rosca, M. Duca, M.T. de Groot, M.T.M. Koper, *Chem. Rev.* 109 (2009) 2209–2244.
- [3] C.J. Pickett, J. Talarmin, *Nature* 317 (1985) 652–653.
- [4] R. Zhang, Y. Zhang, X. Ren, et al., *ACS Sustain. Chem. Eng.* 6 (2018) 9545–9549.
- [5] H. Jia, E.A. Quadrelli, *Chem. Soc. Rev.* 43 (2014) 547–564.
- [6] M. Kitano, Y. Inoue, Y. Yamazaki, et al., *Nat. Chem.* 4 (2012) 934–940.
- [7] K.A. Brown, D.F. Harris, M.B. Wilker, et al., *Science* 352 (2016) 448–450.
- [8] T. Oshikiri, K. Ueno, H. Misawa, *Angew. Chem. Int. Ed.* 55 (2016) 3942–3946.
- [9] G.N. Schrauzer, T.D. Guth, *J. Am. Chem. Soc.* 99 (1977) 7189–7193.
- [10] Z.W. Seh, J. Kibsgaard, C.F. Dickens, et al., *Science* 355 (2017) 1–14.
- [11] L. Wang, M. Xia, H. Wang, et al., *Joule* 2 (2018) 1055–1074.
- [12] T.L. Frolicher, E.M. Fischer, N. Gruber, *Nature* 560 (2018) 360–364.
- [13] Y. Yao, S. Zhu, H. Wang, H. Li, M. Shao, *J. Am. Chem. Soc.* 140 (2018) 1496–1501.
- [14] H.K. Lee, C.S.L. Koh, Y.H. Lee, et al., *Sci. Adv.* 4 (2018) eaar3208.
- [15] J. Kong, A. Lim, C. Yoon, et al., *ACS Sustain. Chem. Eng.* 5 (2017) 10986–10995.
- [16] L. Zhang, X. Ji, X. Ren, et al., *Adv. Mater.* 30 (2018) 1800191.
- [17] S. Chen, S. Perathoner, C. Ampelli, et al., *Angew. Chem. Int. Ed.* 56 (2017) 2699–2703.
- [18] S. Mukherjee, D.A. Cullen, S. Karakalos, et al., *Nano Energy* 48 (2018) 217–226.
- [19] W. Li, T. Wu, S. Zhang, et al., *Chem. Commun.* 54 (2018) 11188–11191.
- [20] L. Huang, J. Wu, P. Han, et al., *Small Methods* 3 (2019) 1800386.
- [21] R. Manjunatha, A. Karajić, V. Goldstein, A. Schechter, *ACS Appl. Mater. Interfaces* 11 (2019) 7981–7989.
- [22] J. Han, X. Ji, X. Ren, et al., *J. Mater. Chem. A* 6 (2018) 12974–12977.
- [23] C. Fang, T. Bi, X. Xu, et al., *Adv. Mater. Interfaces* 6 (2019) 1901034.
- [24] W. Fu, P. Zhuang, M.O. Chee, et al., *ACS Sustain. Chem. Eng.* 7 (2019) 9622–9628.
- [25] I. Nowak, M. Ziolek, *Chem. Rev.* 99 (1999) 3603–3624.
- [26] W. Kong, Z. Liu, J. Han, et al., *Inorg. Chem. Front.* 6 (2019) 423–427.
- [27] J. Han, Z. Liu, Y. Ma, et al., *Nano Energy* 52 (2018) 264–270.
- [28] Y. Huang, Y. Zhang, X. Hu, *Sol. Energy Mater. Sol. C* 77 (2003) 155–162.
- [29] H. Cui, G. Zhu, Y. Xie, et al., *J. Mater. Chem. A* 3 (2015) 11830–11837.
- [30] H. Yu, L. Xu, H. Wang, et al., *Electrochim. Acta* 295 (2019) 829–834.
- [31] M.K. Bahl, *J. Phys. Chem. Solids* 36 (1975) 485–491.
- [32] T. Joshi, T.R. Senty, P. Borisov, A.D. Bristow, D. Lederman, *J. Phys. D Appl. Phys.* 48 (2015) 335308.
- [33] P.L. Searle, *Analyst* 109 (1984) 549–568.
- [34] D. Bao, Q. Zhang, F. Meng, et al., *Adv. Mater.* 29 (2017) 1604799.
- [35] C. Shi, K. Xiang, Y. Zhu, et al., *Electrochim. Acta* 246 (2017) 1088–1096.
- [36] R. Romero, E.A. Dalchiele, F. Martín, D. Leinen, J.R. Ramos-Barrado, *Sol. Energy Mater. Sol. C* 93 (2009) 222–229.